Defining and testing a granular continuum element

Chris H. Rycroft[1,2],* Ken Kamrin[3],† and Martin Z. Bazant[3,4‡]
[1]*Department of Mathematics, Lawrence Berkeley Laboratory, Berkeley, CA 94720, USA*
[2]*Department of Mathematics, University of California, Berkeley, CA 94720, USA*
[3]*Department of Mathematics, Massachusetts Institute of Technology, Cambridge, MA 02139, USA and*
[4]*Physico-Chimie Théorique, Gulliver-CNRS, ESPCI, 10 rue Vauquelin, Paris 75005, France*

Continuum mechanics relies on the fundamental notion of a mesoscopic volume "element" in which properties averaged over discrete particles obey deterministic relationships. Recent work on granular materials suggests a continuum law may be inapplicable, revealing inhomogeneities at the particle level, such as force chains and slow cage breaking. Here, we analyze large-scale Discrete-Element Method (DEM) simulations of different granular flows and show that a "granular element" can indeed be defined at the scale of dynamical correlations, roughly three to five particle diameters. Its rheology is rather subtle, combining liquid-like dependence on deformation rate and solid-like dependence on strain. Our results confirm some aspects of classical plasticity theory (e.g. coaxiality of stress and deformation rate), while contradicting others (i.e. incipient yield), and can guide the development of more realistic continuum models.

Granular materials exhibit many interesting collective phenomena and have attracted growing interest from the physics community [1–4], but many of the central challenges remain unanswered. In particular, there is still no general continuum model that can describe the many phenomena of dense granular flow, such as parabolic flow [5–7] transitioning to plug flow [8] in a draining silo, wide shear zones [9] and localized shear bands [10] in Couette cells, and Bagnold scaling for inclined plane flows [11, 12]. This is in contrast to the hydrodynamics of dilute granular materials and molecular fluids, for which accurate continuum models can be systematically derived by averaging over particle collisions in an idealized element [13].

Recent work has revealed microscopic features of dense granular materials, which seem to defy a simple continuum description. These include: (i) complex, fractal networks of force chains, which are inhomogenous down to the particle level [14–18]; (ii) anomalous, non-collisional particle dynamics with very slow cage breaking [7, 19, 20]; (iii) proximity to the jamming transition, where geometrical packing constraints suppress any dynamics [21, 22]; (iv) a lack of thermal equilibrium in the conventional sense, since particles only move in response to external forces, motivating new definitions of temperature [23–25]; and (v) a wide range of dynamical response, from liquid-like to solid-like [2, 26, 27]. The first four points cast serious doubt on the prospects of a continuum law. The fifth means that the full stress tensor must be described, and it may depend on strain, deformation rate, and material parameters that can evolve during the process.

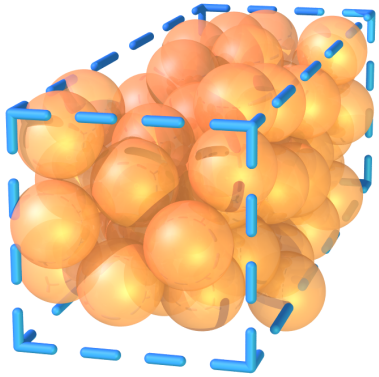

FIG. 1: A typical $2.5d \times 8d \times 2.5d$ cell of particles from a DEM simulation, which forms the basis of the approximate granular element considered in this paper.

We thus arrive at the fundamental question: can a "granular element" be meaningfully defined, and if so, what is its rheology? The oldest definition corresponds to the two-dimensional "Ideal Coulomb Material", in which the granular element behaves like a rigid solid, which undergoes failure if the ratio of shear stress to normal stress in any direction exceeds a critical value μ, the Coulomb internal friction coefficient [28]. The stress tensor is determined by mechanical equilibrium along with the hypothesis of *incipient yield*, which asserts that the yield criterion is attained everywhere at all times (in a "limit state"). In Mohr–Coulomb plasticity, these conditions are assumed to hold even if boundary conditions allow for plastic yielding. In that case, the velocity follows from the assumption of *coaxiality*, which asserts that the stress and deformation rate have the same eigendirections. The resulting equations of Mohr–Coulomb plasticity are used extensively in engineering [28], but their general solution requires sophisticated numerical techniques to capture shock-like discontinuities in stress and velocity, which arise even in relatively simple geometries [29]. Besides the questionable physical basis of such discontinuities, the model is incapable of describing most of the flows listed above,

*Electronic address: chr@math.berkeley.edu
†Electronic address: kenman@mit.edu
‡Electronic address: bazant@mit.edu

even qualitatively.

Recently, a number of theories have been developed to more precisely capture the underlying physics of a granular element. The Shear Transformation Zone theory developed by Langer *et al.* [30, 31] provides a mechanism for the element to retain a memory of its shearing history, through an auxilliary continuum variable, the STZ density. The partial fluidization model of Aranson and Tsimring [26, 27] introduces another auxilliary "order parameter" for the granular element, which controls the size of the viscous-like contribution to the stress tensor. From extensive experimental studies of inclined-plane flows, Jop *et al.* have proposed a 3D flow rule for a granular element at yield [32]. Although each of these models has had successes, none constitutes a complete continuum description of granular flow, which can be applied to more than one of the geometries listed above.

Our group has developed a different, multiscale theoretical framework [19, 20, 33, 34], which, although also not complete, strongly suggests that the length of a granular element is roughly three to five particle diameters (in a dry sphere packing), as shown in Figure 1. This is the typical size of a *spot* of correlated motion among a particle and its nearest neighbors [19], which can be inferred from tracer-diffusion measurements in silo drainage [7, 35]. Independently, the same length scale also emerges from direct measurements of spatial velocity correlations in drainage experiments [36] and DEM simulations [20]. Using this scale in spot-based drainage simulations also produces incredibly realistic flowing random packings [20]. These ideas have also been incorporated into a general theory, which can predict a variety of experimental flow profiles, again using the same length scale (and no other fitting parameters) [33]. Assuming stresses at incipient yield, the coaxial flow rule is be replaced by a "stochastic flow rule" in which spots of mobilized material perform random walks along slip lines, biased by local stress imbalances. The resulting theory is the first to predict both gravity-driven flow in a silo and shear flow in a Couette cell [33, 34], so a major motivation for this work is to directly test its basic assumptions.

By "element", we refer to what is techincally known as a Representative Volume Element (RVE) [37]. An RVE is a mesoscale material volume that is minimal in size but contains enough well-homogenized microconstituents, that a uniform stress state expressed at the RVE boundaries causes a predictable homogeneous boundary deformation and vice versa. Ideally, an RVE is small compared to the macroscopic length of the flow, allowing the material domain to deform as a network of RVEs, each one experiencing close to uniform boundary conditions. Unfortunately, granular flows can form narrow shear bands of width $10d$ to $15d$. Within a band, an RVE would be inhomogenously deformed, reducing the multiplicity of the microstate within, and resulting in a less predictable stress state. Thus, as we study flow relationships at the $3d$ to $5d$ mesoscale, we accept that determinism in any such stress/deformation law will have its limitations.

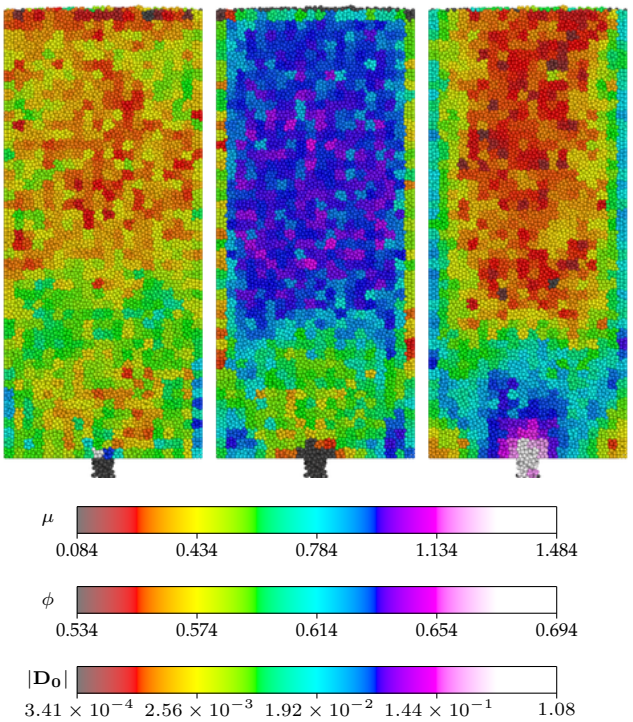

FIG. 2: Three computed material quantities (μ, left; packing fraction ϕ, center; magnitude of deviatoric deformation rate $|\mathbf{D_0}|$, right) in the tall silo drainage simulation, shown at $t = 25\tau$. All the particles in each computational cell are colored according to the computed material parameters for that cell. μ and ϕ are dimensionless, while $|\mathbf{D_0}|$ has units of τ^{-1}.

In this paper, we present the results of several large-scale DEM simulations carried out using the Large-scale Atomic/Molecular Massively Parallel Simulator (LAMMPS) developed by Sandia National Laboratories [38]. The contact model is based on that developed by Cundall and Strack [39], and has been well-tested and used in many other studies [11, 40–42]; details can be found in the Methods section. In the simulations, particles of mass m and diameter d experience gravity g in the negative z direction, which can be used to define a natural time unit $\tau = \sqrt{d/g}$. For the simulations considered here, we restrict attention to cases which are periodic in the horizontal y direction with period $8d$, although this still allows us to consider fully three-dimensional stresses.

Since our overall aim is to extract information about the inherent properties of a granular material, and not its behavior in a particular situation, we consider a variety of granular flows in different geometries. We consider a tall silo with base at $z = 0$ and walls at $x = \pm 25d$, and create an initial packing by pouring in 55000 particles from $z = 160d$ at a constant rate of $123\tau^{-1}$ to fill the silo to an approximate height of $z = 110d$. We also consider a wide silo, with walls at $x \pm 75d, z = 0$, and pour

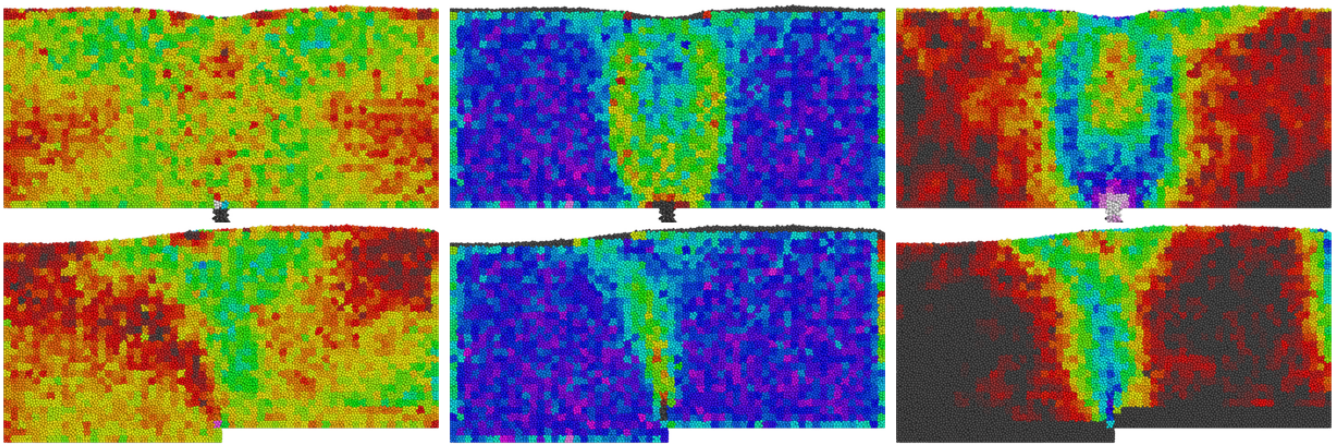

FIG. 3: Three computed material quantities (μ, left; packing fraction ϕ, center; magnitude of deviatoric deformation rate $|\mathbf{D_0}|$, right) in the wide silo for the drainage simulation at $t = 40\tau$ (top) and the pushing simulation at $t = 25\tau$ (bottom). The color scheme used is the same as that in Figure 2.

in 100000 particles from $z = 160d$ at a constant rate of $379\tau^{-1}$. For both situations, the initial packing fraction is approximately 63.5%.

For both packings, a drainage simulation is then carried out, by opening a $6d$-wide slit in the center of the container base. In addition, a pushing simulation is carried out in the wide silo, by freezing all particles whose centers initially satisfy $z < 7.5d$, and then moving those with $x > 0$ upwards at a constant speed of $0.2d\tau^{-1}$. All three of these simulations are quite different in form. The tall silo drainage simulation is different from the wide silo since the velocity profile is strongly affected by the presence of the vertical walls. The pushing simulation corresponds to an active forcing of the material, while the drainage simulations are generated by a passive response to gravity.

For each simulation, a snapshot of all particle positions is recorded at fixed intervals of 0.2τ. In addition to this information, numerous material quantities are calculated in a grid of cells of size $2.5d \times 8d \times 2.5d$, at the scale of the granular element. The local packing fraction ϕ is computed in each cell of interest by evaluating the precise fraction of the cuboidal cell volume which is occupied by the particles. The stress tensor in each cell is calculated by looking at the forces between particles on contact. If there are N particles in the cell, and particle l has a total of N_l contacts, then an approximate stress tensor can be defined as in [43] and simplified for spherical grains to give

$$T_{ij} = \frac{1}{V} \sum_{l=1}^{N} \sum_{k=1}^{N_l} \Delta x_i^{(k,l)} F_j^{(k,l)}$$

where $\mathbf{F}^{(k,l)}$ is the force of the kth contact on particle l, and $\mathbf{\Delta x}^{(k,l)}$ is the separation vector from the center of particle l to its kth contact.

From this, we can define a pressure $p = -\frac{1}{3}\operatorname{tr}\mathbf{T}$ and a deviatoric stress tensor $\mathbf{T_0} = \mathbf{T} + \frac{1}{3}p\mathbf{1}$. To calculate the value of μ, we make use of the classical Mohr–Coulomb definition, in which μ is the ratio of shear stress to normal stress acting on an internal plane of the material element maximized over all possible internal planes. Algebraically, if $\mathbf{T}$ has eigenvalues $\lambda_1 < \lambda_2 < \lambda_3$, then

$$\mu = \frac{\lambda_3 - \lambda_1}{\lambda_3 + \lambda_1}.$$

To calculate the velocity gradient $\mathbf{L}$ in a cell, we consider the least squares regression problem

$$\mathbf{v} = \mathbf{L}\mathbf{x} + \mathbf{v}^0.$$

Here $\mathbf{x}$ and $\mathbf{v}$ are all the instantaneous positions and velocities of all particles within the cell. We find the average cell velocity $\mathbf{v}^0$ and the velocity gradient by minimizing the sum of squares of residuals. The deformation rate tensor is then defined as the symmetric part of $\mathbf{L}$, namely

$$\mathbf{D} = \frac{\mathbf{L} + \mathbf{L}^{\mathrm{T}}}{2}.$$

From this, the deviatoric deformation rate tensor is defined as $\mathbf{D_0} = \mathbf{D} - \frac{1}{3}(\operatorname{tr}\mathbf{D})\mathbf{1}$. In most cases we expect $\mathbf{D_0} \approx \mathbf{D}$ since the density of the granular material does not fluctuate by a large amount, making the contribution to $\mathbf{D}$ from shearing larger than that from dilation. For some of the analysis, we made use of a normalized deformation rate $|\mathbf{I_0}| = |\mathbf{D_0}|d\sqrt{\rho_s/p}$ where ρ_s is the particle density; this has been studied by others [32, 44, 45] and is well-suited for use in rate sensitive granular constitutive laws.

Figure 2 shows plots of μ, ϕ, and $|\mathbf{D_0}|$ for the tall silo drainage simulation. Near the orifice, there is a converging region of flow, that has roughly parabolic streamlines. Higher in the container, there is a transition to

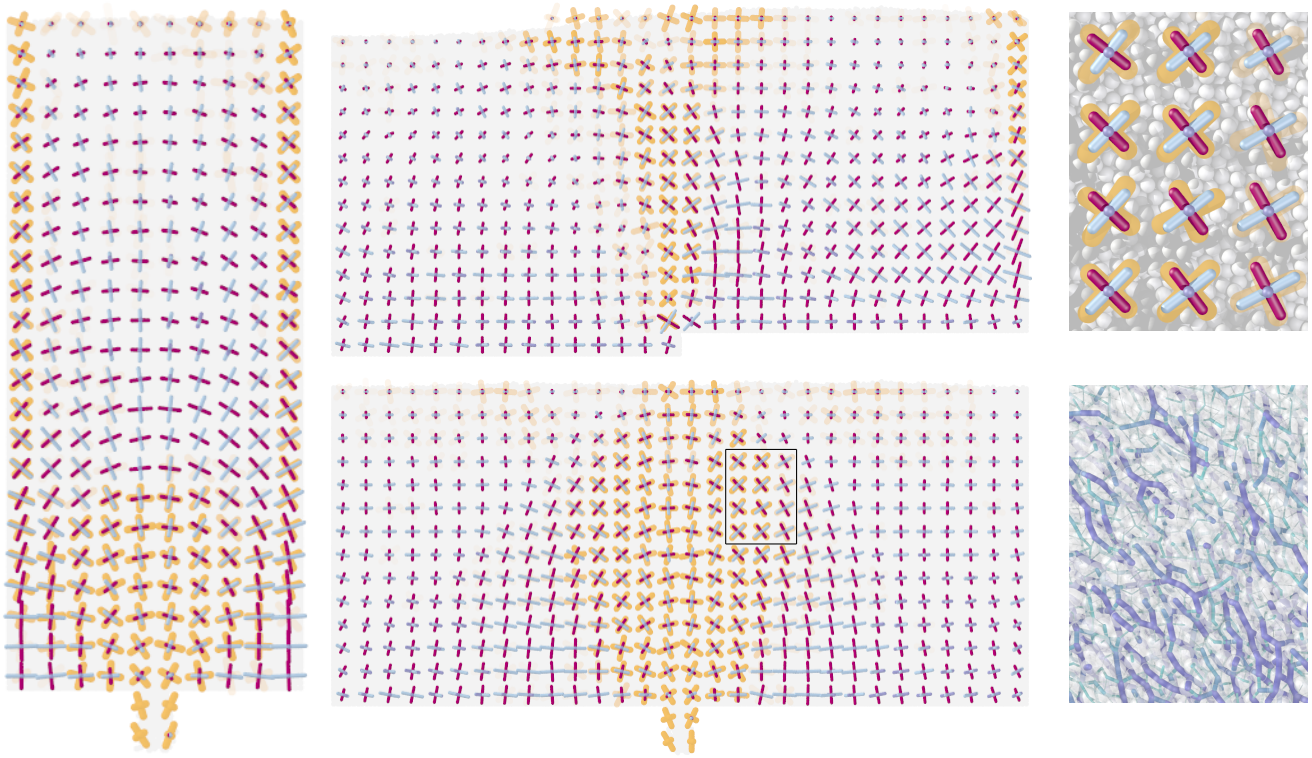

FIG. 4: Plots of the directions and magnitudes of the eigenvectors of the deviatoric stress and deformation rate tensors, calculated instantaneously in $5d \times 8d \times 5d$ boxes with no time-averaging. The maximal stress eigenvector is shown in purple, with the other two eigenvectors being shown in blue. In the regions where deformation is occurring, the maximal and minimal eigenvectors of the deformation rate tensors are plotted in orange. In all cases, a high degree of alignment between the two tensors can be seen. The top right panel shows a detail from the wide drainage simulation, while the bottom right panel shows the individual forces between the particles in the same region. Additional plots are available in the Supplementary Information.

uniform flow, where the particles drop like a plug, behave like a solid, and experience little rearrangement, as has been seen in similar situations [8]. The plot of $|\mathbf{D_0}|$ supports these results. High in the container, very little rearrangement is seen, while there is a sharp transition to high values when the packing must undergo deformation to pass through the orifice.

It is clear from the plots that ϕ and $|\mathbf{D_0}|$ are closely correlated. In the upper region, where particles are falling like a plug, the packing fraction remains constant. In the converging region, the packing fraction decreases, as the particles must have more free space in order to geometrically rearrange; this is studied quantitatively later.

Of the three plots, μ exhibits the largest fluctuations, which we attribute to the fact that it is a ratio between two computed quantities. However, large variations over the range 0.2 to 0.6 can be clearly seen. This immediately calls the Mohr–Coulomb incipient yield hypothesis into question, which would predict that μ would be constant everywhere. At first sight, the spatial differences in μ appear not directly correlated with the other two. However, regions of higher μ exist at the interface between the plug-like region, and the converging flow region; this will be expanded on later. Figure 3 shows the same three plots for the wide drainage and wide pushing simulations, and the same relationships between the three quantities can be observed.

Figure 4 shows the directions and magnitudes of the eigenvectors of the deviatoric stress tensor for three different situations. For these images, the stress tensor was calculated on a $5d \times 8d \times 5d$ grid, by averaging the computed stress tensor in 2×2 blocks of cells. Even though they were computed using local, instantaneous data, we can see that in all situations, the stress tensors are smooth, and exhibit none of the shocks predicted by limit-state plasticity theory. For regions undergoing deformation, the eigenvectors of $\mathbf{D_0}$ are also shown in Figure 4. We see that in all areas where there is appreciable deformation rate, there is a strong alignment between the two sets of eigenvectors. At this scale, the average angular differential between the maximal eigenvectors is approximately $12°$. If the plots are time-averaged over a window of twenty frames, then the mean angular differential drops to $6.7°$. Averaging over progressively larger time windows also allows us to verify coaxiality as far into the granular packing as one can reasonably define a deformation rate tensor. Coaxiality is a consequence of material isotropy at the scale of a contin-

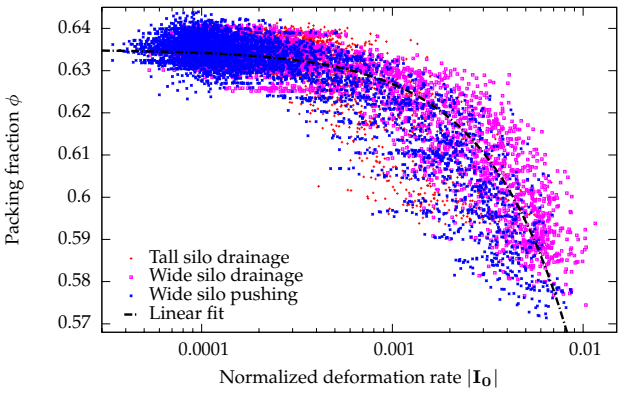

FIG. 5: A plot of packing fraction ϕ versus normalized deformation rate $|\mathbf{I_0}|$. Each point corresponds to the computed material quantities for a granular element from one of the three DEM simulations.

uum element, so it appears that increasing the time window increases the extent to which the liquid-like material flows like a true continuous fluid.

Using this data, we tested the codirectionality hypothesis $\mathbf{T_0} \propto \mathbf{D_0}$. This assertion is stronger than just coaxiality and has been presumed by some [32] while challenged by others [46]. Our data reveals reasonably large variations from purely codirectional flow. It is possible that double-shearing [47] may be a more appropriate hypothesis, but more testing is necessary.

We now investigate quantitatively the connections seen above, by viewing all the material cells from the different simulations as an ensemble of approximate "granular elements", and seeking statistical relationships between them. As a first example, consider Figure 5, showing a plot of $|\mathbf{I_0}|$ against ϕ. Each point on the graph corresponds to the instantaneous computed values of a material element from one of the simulations, during a period when steady flow has developed. We see an approximate collapse of the points from the three simulations, suggesting that the correlation we are viewing is a property inherent to the granular material, and not tied to any particular simulation configuration. Also shown is a fit line $|\mathbf{I_0}| = 0.123(\rho - 0.635)$, The linear relationship is consistent with the two-dimensional results of da Cruz [44].

While instructive, the above approach will only allow us to search for direct correlations between variables. In reality, we expect that the material parameters are related in a more complicated way, and that differential relationships may exist; there may also be internal state variables which we are not measuring, that relate to an element's history of deformation and stress. Because of these complications, it is natural to switch from an Eulerian to Lagrangian approach: rather than viewing our data set as an ensemble over fixed spatial positions, we treat it as an ensemble of material elements which deform and move with the flow. Each granular element corresponds to an approximate trace in the phase space of material parameters over its history during the simulation.

To correctly implement this, we must also take into account that a granular cell may move during the simulation. We therefore initially introduced a number of tracer positions on a $5d \times 5d$ lattice. During the simulation, the tracer positions are advected according the average background velocity of the particles. For each tracer, a history of a granular element is created by linearly interpolating all the material parameters from the underlying raw simulation data on the $2.5d \times 2.5d$ lattice.

Figure 6(a) shows material tracers in a plot of μ versus ϕ for the three different simulations. The plot shows us that, while μ is not directly correlated to ϕ, it plays an important role in the failure of a granular element. The majority of tracers start off on the right side of the graph, at the initial packing fraction of 63.5%. Those tracers corresponding to failing elements take a path in an inverted U-shape, first attaining a value of μ of approximately 0.6 before starting to decrease in packing fraction. A material element will dilate only if a critical value of μ is first attained. This directly relates to the behavior seen in Figures 2 and 3, where it was noted that areas of larger μ were located at the interface between solid-like and liquid-like regions. Also visible in 6(a) is a tendency for dilated elements which experience a low value of μ to recompact slightly.

The Lagrangian approach also allows us to get a clearer insight into shear dilation, the precise mechanics of which remains an open study. Our results showed correlations between packing fraction and deformation rate, in agreement with other authors. However, there are also numerous examples in the literature of "rate-independent" plasticity [48–50] which propose that the total strain is instrumental in determining the amount of dilation. Since one would expect for a single snapshot, the regions of high strain could roughly be correlated with the regions of high deformation rate, we defer to a quantitative analysis to attempt to resolve this paradox.

Strain is calculated from the simulation data by using the snapshots of all particle positions. At $t = 0$, a $5d \times 8d \times 5d$ box of particles is labeled, centered on each material tracer. Let $\mathbf{x}^i$ be the initial particle positions in a particular box. A deformation gradient tensor $\mathbf{F}$ and an overall translation $\mathbf{x}^0$ can then be found by solving the least squares regression problem

$$\mathbf{x} = \mathbf{F}\mathbf{x}^i + \mathbf{x}^0$$

where $\mathbf{x}$ are the current particle positions. We then compute the polar decomposition $\mathbf{F} = \mathbf{R}\mathbf{U}$ where $\mathbf{R}$ is a rotation matrix, and the stretch $\mathbf{U}$ is a symmetric positive definite matrix. Unlike infinitessimal theory, there are many valid ways to define the strain tensor for large deformations, though each way must be a function of $\mathbf{U}$ which asymptotes under small stretches to the well-known infinitessimal definition. Here, we choose the Hencky strain measure $\mathbf{E} \equiv \log \mathbf{U}$, which has the ad-

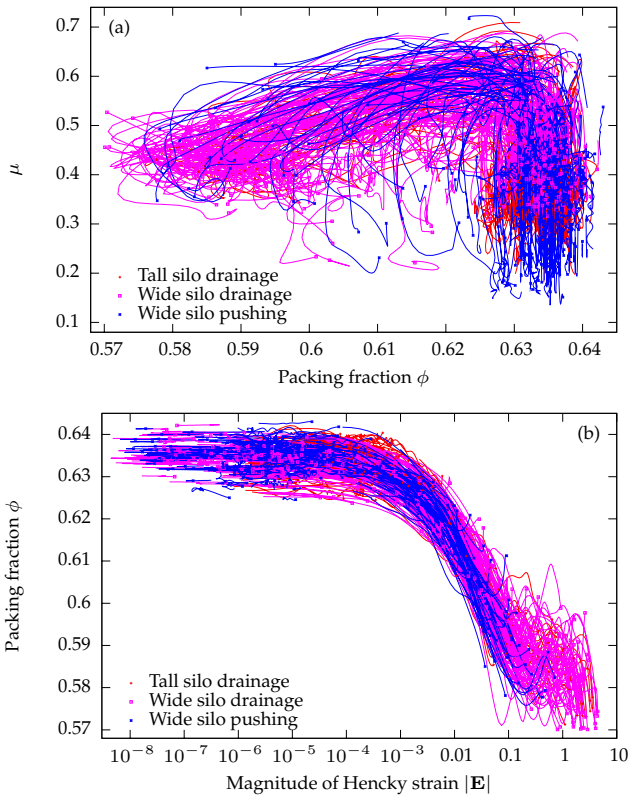

FIG. 6: Lagrangian tracer plots of (a) μ versus packing fraction ϕ and (b) packing fraction ϕ versus magnitude of Hencky strain $|\mathbf{E}|$. Each line corresponds to the trace in phase space of a granular element.

ditional property that strains are additive in the absence of rotation.

Figure 6(b) shows a plot of packing fraction versus strain, with a sharp collapse of the trajectories across several simulations. In order to be consistent with Figure 5, strain must be instrumental in the process by which the material dilates, but deformation rate sets the final packing fraction.

The above results show that it is possible to make a direct connection between continuum theories and particle-based simulations of dense granular flow at the local level. Motivated by previous work on co-operative particle motion, we have shown that it is possible to define an approximate granular element at the level of several particle diameters, and while material quantities computed at this scale exhibit statistical variation, they are clear enough to test the rheology of granular materials. Our simulations are consistent with some previous numerical studies [44, 46], but we have been able to show these results locally and instantaneously in several different three-dimensional geometries.

In the future we hope to directly evaluate the some of the recently proposed theories for granular materials [26, 30, 32]. These are frequently characterized by having a microscopic continuum quantity, such as STZ populations $n_\pm$ or partial fluidization parameter ρ, and part of the challenge in investigating these parameters will be to understand how they directly relate to the microscopic packing structure. Another promising avenue to pursue is to better understand the role of total strain. While strain appeared to play a crucial role in interpreting our data, it is an undesirable quantity to use in an eventual continuum theory of granular materials, since it is always tied to an initial reference state. Examining fully 3D situations may also provide useful clues, since it may allow us greater control and variation in the stress tensor. In this work, we only considered yielding as a function of μ, which is defined in terms of the maximum and minimum stress eigenvalue. A useful study would be to check the role, if any, of the intermediate stress eigenvalue, a question which is currently unresolved.

Methods

Particles are modeled as frictional, visco-elastic glass beads of diameter d and mass m, and interact according to Hookean, history dependant contact forces. If a particle an its neighbor have a separation vector $\mathbf{r}$, and the two particles are in contact, so that $\delta = d - |\mathbf{r}| > 0$, then they experience a force $\mathbf{F} = \mathbf{F}_n + \mathbf{F}_t$, where the normal and tangential components are given by

$$\begin{aligned} \mathbf{F}_n &= \left(k_n \delta \mathbf{n} - \frac{\gamma_n \mathbf{v}_n}{2}\right) \\ \mathbf{F}_t &= \left(-k_t \Delta \mathbf{s}_t - \frac{\gamma_t \mathbf{v}_t}{2}\right). \end{aligned}$$

Here, $\mathbf{n} = \mathbf{r}/|\mathbf{r}|$. $\mathbf{v}_n$ and $\mathbf{v}_t$ are the normal and tangential components of the relative surface velocity, and $k_{n,t}$ and $\gamma_{n,t}$ are the elastic and viscoelastic constants, respectively. $\Delta \mathbf{s}_t$ is the elastic tangential displacement between spheres, obtained by integrating tangential relative velocities during elastic deformation for the lifetime of the contact, and is truncated as necessary to satisfy a local Coulomb yield criterion $|\mathbf{F}_t| \leq \mu |\mathbf{F}_n|$. Particle–wall interactions are treated identically, but the particle–wall friction coefficient is set independently. For the current simulations we set $k_t = \frac{2}{7} k_n$, and choose $k_n = 2 \times 10^5 mg/d$. While this is significantly less than would be realistic for glass spheres, where we expect $k_n \sim 10^{10} mg/d$, such a spring constant would be prohibitively computationally expensive, as the time step must have the form $\delta t \propto k_n^{-1/2}$ for collisions to be modeled effectively. Previous simulations have shown that increasing k_n does not significantly alter physical results [40]. We make use of a time step of $\delta t = 1.75 \times 10^{-6}$s, and damping coefficients $\gamma_n = \gamma_t = 50\sqrt{g/d}$.

[1] H. M. Jaeger and S. R. Nagel, Science **255**, 1523 (1992).
[2] H. M. Jaeger, S. R. Nagel, and R. P. Behringer, Rev. Mod. Phys. **68**, 1259 (1996).
[3] P. G. de Gennes, Rev. Mod. Phys. **71**, S374 (1999).

[4] T. Halsey and A. Mehta, eds., *Challenges in Granular Physics* (World Scientific, 2002).
[5] A. Medina, J. A. Cordova, E. Luna, and C. Trevino, Physics Letters A **220**, 111 (1998).
[6] R. M. Nedderman and U. Tüzün, Powder Technology **22**, 243 (1979).
[7] J. Choi, A. Kudrolli, R. R. Rosales, and M. Z. Bazant, Phys. Rev. Lett. **92**, 174301 (2004).
[8] C. H. Rycroft, G. S. Grest, J. W. Landry, and M. Z. Bazant, Phys. Rev. E **74**, 021306 (2006).
[9] D. Fenistein and M. van Hecke, Nature **425**, 256 (2003).
[10] D. M. Mueth, Phys. Rev. E. **67**, 011304 (2003).
[11] L. E. Silbert, D. Ertaş, G. S. Grest, T. C. Halsey, D. Levine, and S. J. Plimpton, Phys. Rev. E **64**, 051302 (2001).
[12] O. Pouliquen, Phys. Fluids **11**, 542 (1999).
[13] J. T. Jenkins and S. B. Savage, J. Fluid Mech. **130**, 187 (1983).
[14] D. M. Mueth, H. M. Jaeger, and S. R. Nagel, Phys. Rev. E **57**, 3164 (1998).
[15] D. L. Blair, N. Mueggenburg, A. M. Marshall, H. M. Jaeger, and S. R. Nagel, Phys. Rev. E **63**, 041304 (2001).
[16] S. F. Edwards, Physica A **249**, 226 (1998).
[17] C. h. Liu, S. R. Nagel, D. A. Schecter, N. Coppersmith, S. Majumdar, O. Narayan, and T. A. Witten, Science **269**, 513 (1995).
[18] T. S. Majumdar and R. P. Behringer, Nature **435**, 1079 (2005).
[19] M. Z. Bazant, Mechanics of Materials **38**, 717 (2006).
[20] C. H. Rycroft, M. Z. Bazant, G. S. Grest, and J. W. Landry, Phys. Rev. E **73**, 051306 (2006).
[21] C. S. O'Hern, L. E. Silbert, A. J. Liu, and S. R. Nagel, Phys. Rev. E **68**, 011306 (2003).
[22] A. Donev, S. Torquato, F. H. Stillinger, and R. Connelly, J. Appl. Phys. **95**, 989 (2004).
[23] S. Henkes, C. S. O'hern, and B. Chakraborty, Phys. Rev. Lett. **99**, 10.1103/PhysRevLett.99.038002 JUL 20 2007 (2007).
[24] S. F. Edwards and D. V. Grinev, Phys. Rev. E **58**, 4758 (1998).
[25] H. A. Makse and J. Kurchan, Nature **415**, 614 (2002).
[26] I. S. Aranson and L. S. Tsimring, Phys. Rev. E **64**, 020301 (2001).
[27] I. S. Aranson and L. S. Tsimring, Phys. Rev. E **65**, 061303 (2002).
[28] R. M. Nedderman, *Statics and Kinematics of Granular Materials* (Nova Science, 1991).
[29] P. A. Gremaud and J. V. Matthews, J. Comput. Phys. **166**, 63 (2001).
[30] M. L. Falk and J. S. Langer, Phys. Rev. E **57**, 7192 (1998).
[31] A. Lemaître, Phys. Rev. Lett. **89**, 195503 (2002).
[32] P. Jop, Y. Forterre, and O. Pouliquen, Nature **441**, 727 (2006).
[33] K. Kamrin and M. Z. Bazant, Phys. Rev. E **75**, 041301 (2007), cond-mat/0609448.
[34] K. Kamrin, C. H. Rycroft, and M. Z. Bazant, Modelling Simul. Mater. Sci. Eng. **15**, S449 (2007).
[35] J. Choi, A. Kudrolli, and M. Z. Bazant, J. Phys.: Condensed Matter **17**, S2533 (2005).
[36] J. Choi, Ph.D. thesis, Massachusetts Institute of Technology (2005).
[37] Z. Hashin, J. Appl. Mech. **50**, 481 (1983).
[38] http://lammps.sandia.gov/.
[39] P. A. Cundall and O. D. L. Strack, Geotechnique **29**, 47 (1979).
[40] J. W. Landry, G. S. Grest, L. E. Silbert, and S. J. Plimpton, Phys. Rev. E **67**, 041303 (2003).
[41] L. E. Silbert, G. S. Grest, and J. W. Landry, Phys. Rev. E **66**, 061303 (2002).
[42] R. C. Brewster, J. W. Landry, G. S. Grest, and A. J. Levine, Phys. Rev. E **72**, 061301 (2005).
[43] J. Christoffersen, M. M. Mehrabadi, and S. Nemat-Nasser, J. Appl. Mech. **48**, 339 (1981).
[44] F. da Cruz, S. Emam, M. Prochnow, J. Roux, and F. Chevoir, Phys. Rev. E. **72**, 021309 (2005).
[45] G. Lois, A. Lemaitre, and J. M. Carlson, Phys. Rev. E. **72**, 051303 (2005).
[46] M. Depken, J. B. Lechman, M. van Hecke, W. van Saarloos, and G. S. Grest, Europhys. Lett. **78**, 58001 (2007).
[47] A. J. M. Spencer, J. Mech. Physics **12**, 337351 (1964).
[48] A. Schofield and C. Wroth, *Critical State Soil Mechanics* (McGraw-Hill, 1968).
[49] J. W. Rudnicki and J. R. Rice, J. Mech. Phys. Solids **23**, 371 (1975).
[50] L. Anand and C. Gu, J. Mech. Phys. Solids **28**, 1701 (2000).

Acknowledgments

This work was supported by the Director, Office of Science, Computational and Technology Research, U.S. Department of Energy under Contract Nos. DE-AC02-05CH11231 and DE-FG02-02ER25530; and also by the Norbert Weiner Research Fund and the NEC Fund at MIT.

Defining and testing a granular continuum element: supplementary figures

Chris H. Rycroft, Ken Kamrin, and Martin Z. Bazant

December 3, 2007

Description

This document contains additional plots of the stress and deformation rate tensors to supplement those in figure 4 of the paper. For each situation, the stress and deformation rate tensors are calculated in $5d \times 8d \times 5d$ boxes, using instantaneous information, with no time-averaging. The maximal stress eigenvector is shown purple, and the other two eigenvectors are shown in blue. The length of each component is proportional to the square root of the magnitude of the deviatoric stress eigenvalue. In the regions where deformation is occurring, the maximal and minimal eigenvectors of the deformation rate tensors are plotted in orange.

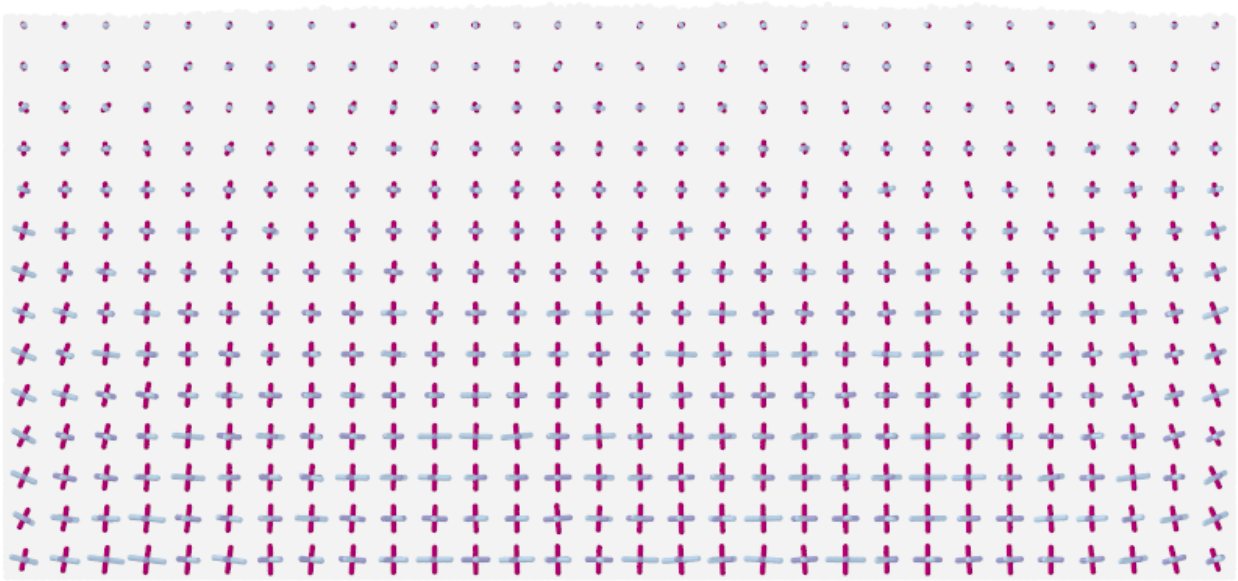

Figure S1: Plots of the directions and magnitudes of the eigenvectors of the deviatoric stress tensors for the wide initial packing.

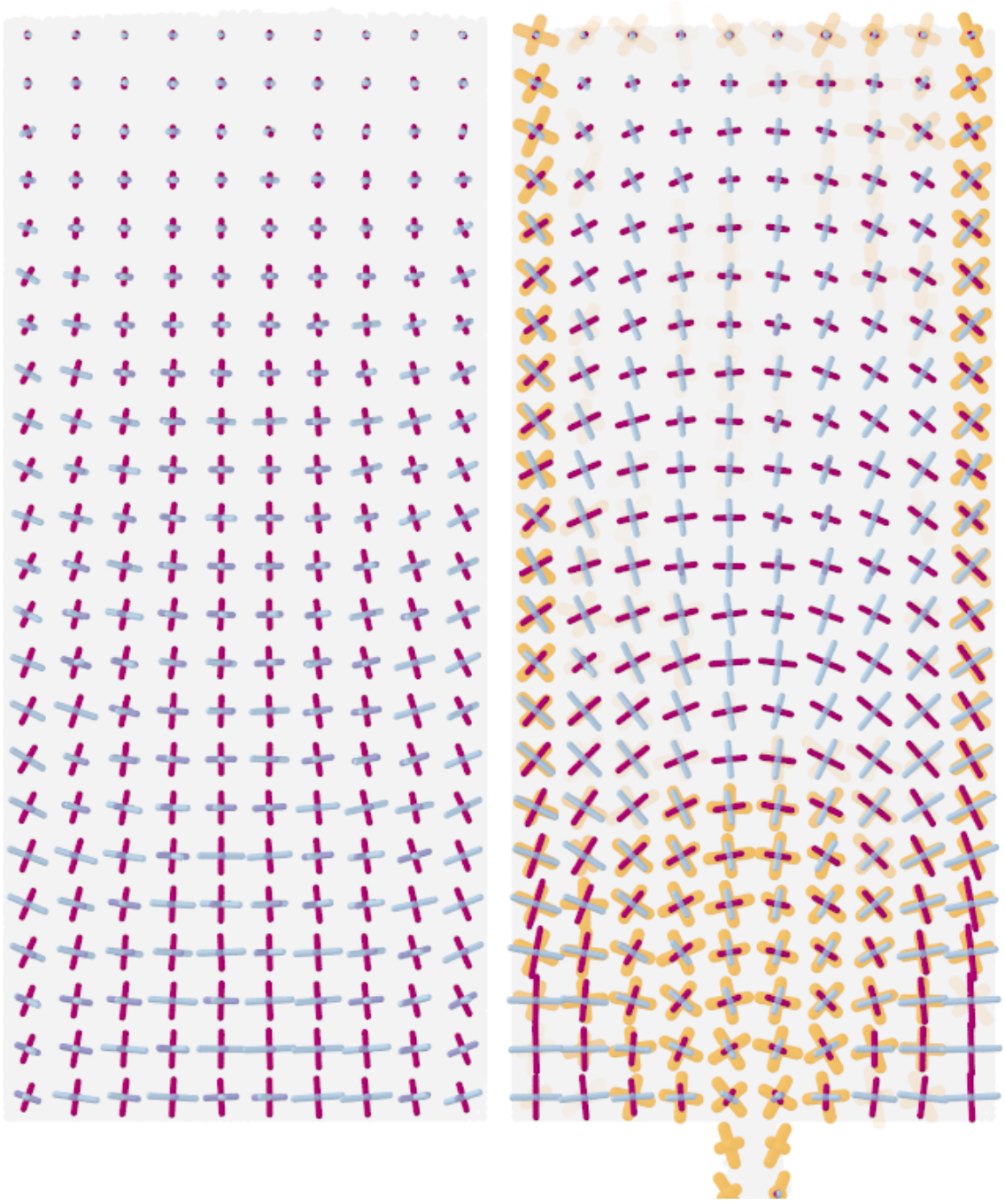

Figure S2: Plots of the directions and magnitudes of the eigenvectors of the deviatoric stress and deformation rate tensors for the tall silo before drainage (left), and during drainage (right). During drainage, a high degree of alignment between the two tensors can be seen.

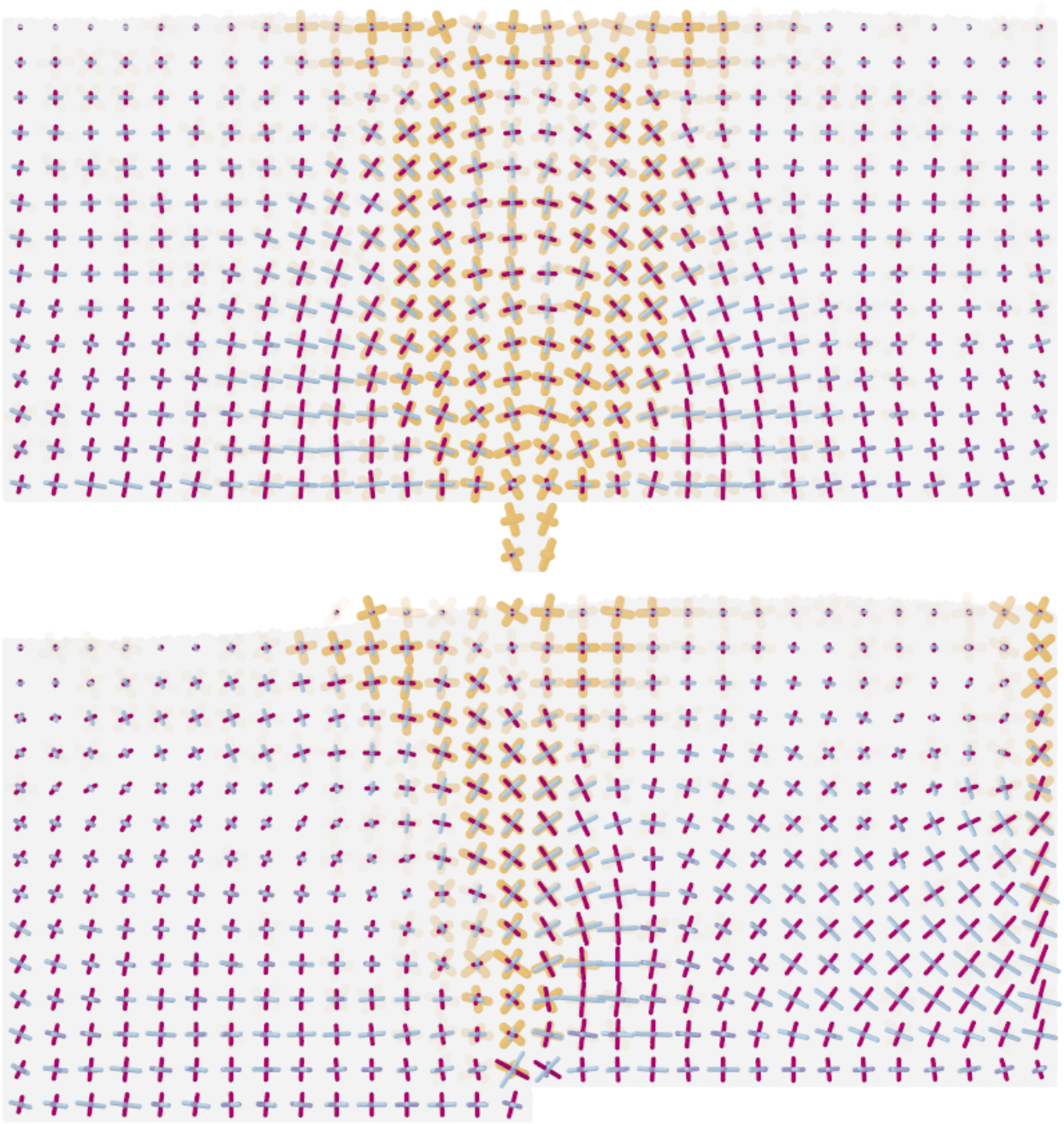

Figure S3: Plots of the directions and magnitudes of the eigenvectors of the deviatoric stress and deformation rate tensors for the wide granular packing during drainage (top), and during pushing (bottom). Again, a high degree of alignment between the two tensors can be seen.

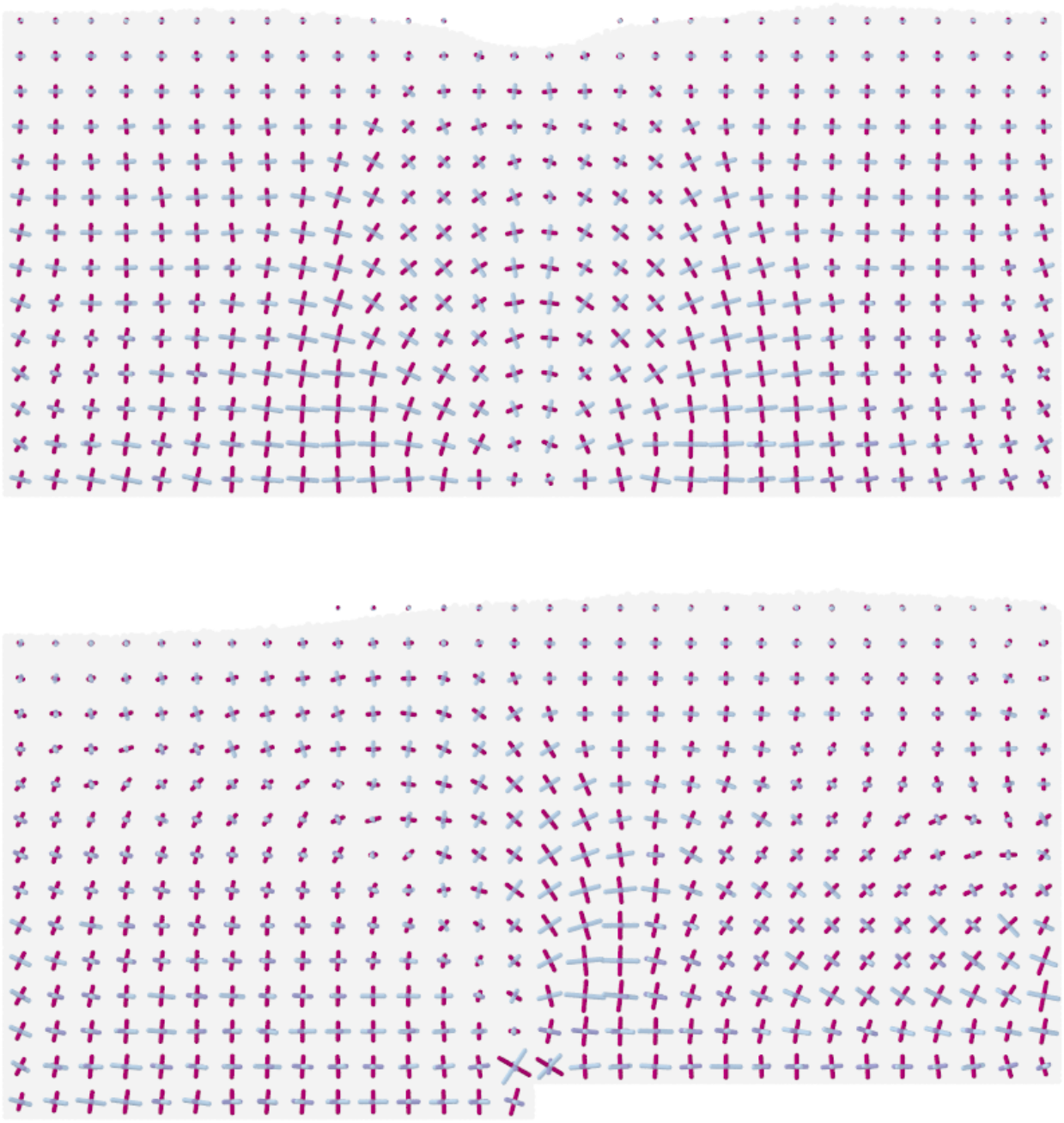

Figure S4: Plots of the directions and magnitudes of the eigenvectors of the deviatoric stress tensors after the drainage (top) and pushing processes (bottom) were arrested. The stress lines closely resemble those in the corresponding flowing states.